PROCEEDINGS OF SCIENCE

Fluctuation of the initial condition from Glauber models*

Wojciech Broniowski†
Institute of Physics, Świętokrzyska Academy, PL-25406 Kielce, Poland, and
The H. Niewodniczański Institute of Nuclear Physics, PL-31342 Kraków, Poland
E-mail: Wojciech.Broniowski@ifj.edu.pl

Piotr Bożek
The H. Niewodniczański Institute of Nuclear Physics, PL-31342 Kraków, Poland, and
Institute of Physics, Rzeszów University, PL-35959 Rzeszów, Poland
E-mail: Piotr.Bozek@ifj.edu.pl

Maciej Rybczyński
Institute of Physics, Świętokrzyska Academy, PL-25406 Kielce, Poland
E-mail: Maciej.Rybczynski@pu.kielce.pl

We analyze measures of the azimuthal asymmetry, in particular the *participant* harmonic moments, ε^*, in a variety of Glauber-like models for the early stage of collisions at RHIC. Quantitative comparisons indicate substantial model dependence for ε^*, reflecting different effective number of sources, while the dependence of the scaled standard deviation $\sigma(\varepsilon^*)/\varepsilon^*$ on the particular Glauber model is weak. For all the considered models the values of $\sigma(\varepsilon^*)/\varepsilon^*$ range from ~ 0.5 for the central collisions to $\sim$ 0.3-0.4 for peripheral collisions. These values, dominated by statistics, change only by 10-15% from model to model. For central collisions and in the absence of correlations between the location of sources we obtain through the use of the central limit theorem the simple analytic formula $\sigma(\varepsilon^*)/\varepsilon^*(b=0) \simeq \sqrt{4/\pi - 1} \simeq 0.52$, independent on the collision energy, mass number, or the number of sources. In consequence, with smooth hydrodynamics at central collisions $\sigma(v_2)/v_2(b=0) \simeq \sqrt{4/\pi - 1}$. We show, that the same value is achieved also at *peripheral* collisions, as long as the particles come from a collection of independent pp collisions. We investigate the shape-fluctuation effects on jet quenching and find they are important only for very central events. Finally, we list some remarks and predictions from smooth hydrodynamics on higher flow coefficients and their fluctuations, in particular $\sigma(v_4)/v_4 = 2\sigma(v_2)/v_2$.

Critical Point and Onset of Deconfinement 4th International Workshop
July 9-13 2007
GSI Darmstadt,Germany

*Supported by Polish Ministry of Science and Higher Education under grants N202 034 32/0918 and 2 P03B 02828.
†Speaker.

PoS(CPOD07)014

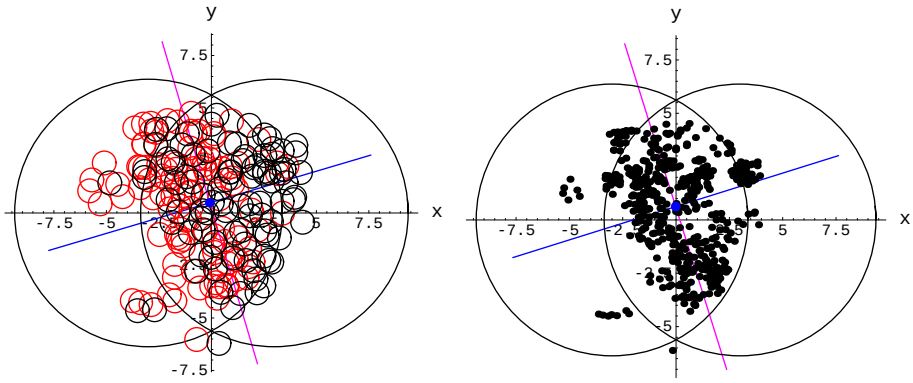

Figure 1: A typical gold-gold collision in the $x-y$ plane at $b = 6$ fm. Left: wounded nucleons. Red and black circles indicate nucleons from the two colliding nuclei. Right: the centers of mass of pairs of nucleons undergoing binary collisions. The straight lines indicate the twisted and shifted principal axes of the second harmonic moment, while the blue dots show the center of mass of the system.

1. Introduction

This talk is based on Ref. [1], where more technical details may be found.

Event-by-event hydrodynamic studies [2, 3] of relativistic heavy-ion collisions have revealed that *fluctuations of the initial shape* of the system formed in the early stage of the reaction lead to quantitatively relevant effects for signatures of the azimuthal asymmetry [4, 5, 6, 7, 8]. These effects are also important for experimental measurements of the elliptic flow [9, 10, 11, 12]. In this talk we report our investigation of this phenomenon in the framework of various Glauber-like approaches describing the deposition of energy in the system in the early stages of the collision. Our study focuses on both understanding of the statistical nature of the results, as well as on comparisons of various models.

Figure 1 illustrates the two effects of the shape fluctuations due to the finite number of sources: the shift of the center-of-mass and the rotation of the principal axes. Statistical analyses may be performed in the reference frame fixed by the reaction plane (we call it *fixed-axes*, a.k.a. standard), or for each event in the frame defined by the twisted and shifted principal axes (we call it the *variable-axes* frame, a.k.a. participant). In the fixed-axes frame the two-dimensional probability distribution of sources can be Fourier-expanded as

$$f(\rho,\phi) = f_0(\rho) + 2f_2(\rho)\cos(2\phi) + 2f_4(\rho)\cos(4\phi) + \ldots, \tag{1.1}$$

where the transverse radius $\rho = \sqrt{x^2+y^2}$ is measured from the center of the geometric intersection of the two nuclei. One also introduces

$$\varepsilon_l = \frac{\int 2\pi\rho\, f_l(\rho)\rho^2 d\rho}{\int 2\pi\rho\, f_0(\rho)\rho^2 d\rho}. \tag{1.2}$$

On the other hand, in the variable-axes frame we have the distribution

$$f^*(\rho,\phi) = f_0(\rho) + 2f_2^*(\rho)\cos(2\phi - 2\phi^*) + 2f_4^*(\rho)\cos(4\phi - 4\phi^*) + \ldots, \tag{1.3}$$

where ϕ^* denotes the rotation angle of the principal axes in each event. Correspondingly,

$$\varepsilon_l^* = \frac{\int 2\pi\rho\, f_l^*(\rho)\rho^2 d\rho}{\int 2\pi\rho\, f_0(\rho)\rho^2 d\rho} \tag{1.4}$$

($f_0 = f_0^*$). The deformation parameters are denoted without the subscript as $\varepsilon = \varepsilon_2$ and $\varepsilon^* = \varepsilon_2^*$.

2. The toy problem

Consider the one-dimensional problem where uncorrelated particles are randomly generated from a distribution in the azimuthal angle ϕ containing the zeroth and second harmonic moments,

$$f(\phi) = 1 + 2\varepsilon\cos(2\phi), \quad \varepsilon \in [-\frac{1}{2}, \frac{1}{2}]. \tag{2.1}$$

Obviously, the distribution has only two non-zero fixed-axes moments,

$$f_0 = \frac{1}{2\pi}\int_0^{2\pi} d\phi\, f(\phi) = 1, \quad f_2 = \frac{1}{2\pi}\int_0^{2\pi} d\phi\cos(2\phi) f(\phi) = \varepsilon. \tag{2.2}$$

We generate n particles according to the distribution (2.1) in each event, and subsequently carry out the averaging over the events, denoted as $\langle\langle . \rangle\rangle$. For instance, f_2 is estimated as

$$f_2 \simeq \langle\langle \frac{1}{n}\sum_{k=1}^{n}\cos(2\phi_k)\rangle\rangle, \tag{2.3}$$

where k labels the particles the event. The equality becomes strict as the number of events approaches infinity, which is assumed implicitly. In the variable-axes case we rotate the particles by the angle ϕ^* in each event. Thus

$$f_2^* \equiv \varepsilon^* = \langle\langle \frac{1}{n}\sum_{k=1}^{n}\cos[2(\phi_k - \phi^*)]\rangle\rangle. \tag{2.4}$$

The rotation angle ϕ^* depends itself on the distribution of particles in the given event. By definition, it is chosen in such a way that the quantity $\frac{1}{n}\sum_{k=1}^{n}\cos[2(\phi_k - \phi^*)]$ assumes maximum, which gives the conditions

$$\begin{aligned} &\cos(2\phi^*) = Y_2/\sqrt{Y_2^2 + X_2^2}, \quad \sin(2\phi^*) = X_2/\sqrt{Y_2^2 + X_2^2}, \\ &Y_2 = \frac{1}{n}\sum_{k=1}^{n}\cos(2\phi_k), \quad X_2 = \frac{1}{n}\sum_{k=1}^{n}\sin(2\phi_k). \end{aligned} \tag{2.5}$$

Using the above formulas in Eq. (2.4) yields

$$f_2^* = \langle\langle\sqrt{Y_2^2 + X_2^2}\rangle\rangle = \langle\langle\sqrt{\left(\frac{1}{n}\sum_{k=1}^{n}\cos(2\phi_k)\right)^2 + \left(\frac{1}{n}\sum_{k=1}^{n}\sin(2\phi_k)\right)^2}\,\rangle\rangle. \tag{2.6}$$

We see that the variable-axes moment corresponds to an average of the square root of sums (2.5), thus is a highly "non-local" object, involving upon expansion infinitely many fixed-axes moments.

For sufficiently large n one may evaluate Eq. (2.6) with the help of the *central limit theorem*. Consider the variables $c_k = \cos(2\phi_k)$ and $s_k = \sin(2\phi_k)$. Their averages and variances are

$$\bar{c} = \varepsilon, \;\; \sigma_c^2 = \frac{1}{2} - \varepsilon^2, \;\; \bar{s} = 0, \;\; \sigma_s^2 = \frac{1}{2}. \tag{2.7}$$

Importantly, there is no correlation between Y_2 and X_2, as $\frac{1}{2\pi}\int_0^{2\phi} d\phi \cos(2\phi)\sin(2\phi) f(\phi) = 0$. Thus, according to the central limit theorem, the distribution of Y_2 and X_2 is Gaussian. Introducing

$$Y_2 = q\cos\alpha, \quad X_2 = q\sin\alpha, \quad q^2 = Y_2^2 + X_2^2, \quad \delta = \frac{1}{2\sigma_c^2} - \frac{1}{2\sigma_s^2} = \frac{1}{1-2\varepsilon^2} - 1, \tag{2.8}$$

we may write this distribution in the form

$$f(X_2, Y_2) = f(q,\alpha) = \frac{n}{\pi\sqrt{1-2\varepsilon^2}} \exp\left[-n\left(\frac{q^2+\varepsilon^2 - 2q\varepsilon\cos\alpha}{1-2\varepsilon^2}\right) + n\delta q^2 \sin^2\alpha\right]. \tag{2.9}$$

We need below the integral of this distribution over α, which can be expanded as [13, 11]

$$\int_0^{2\pi} d\alpha\, f(q,\alpha) = \frac{2n}{\sqrt{\pi}\sqrt{1-2\varepsilon^2}} \exp\left[-n\left(\frac{q^2+\varepsilon^2}{1-2\varepsilon^2}\right)\right] \sum_{j=0}^{\infty} (2q\varepsilon)^j \frac{\Gamma(j+\frac{1}{2})}{j!} I_j\left(\frac{2n\varepsilon q}{1-2\varepsilon^2}\right), \tag{2.10}$$

where $I_j(x)$ are the modified Bessel functions. We may now express Eq. (2.4) as the series involving the confluent hypergeometric function,

$$f_2^* = \int q\,dq\,d\alpha\, q f(q,\alpha) = \frac{1-2\varepsilon^2}{\sqrt{n\pi}} \sum_{j=0}^{\infty} \left(2\varepsilon^2\right)^j \frac{\Gamma(j+\frac{1}{2})\Gamma(j+\frac{3}{2})}{j!^2} {}_1F_1\left(-\frac{1}{2}, j+1; -\frac{n\varepsilon^2}{1-2\varepsilon^2}\right), \tag{2.11}$$

which converges fast and can be used for practical calculations in a truncated form. At $\varepsilon = 0$ (azimuthally symmetric distribution) we have the very simple result

$$f_2^*(\varepsilon = 0) = \frac{\sqrt{\pi}}{2\sqrt{n}}, \tag{2.12}$$

which shows the expected $1/\sqrt{n}$ behavior for a statistical fluctuation. The numerical results obtained with the series (2.11) are presented in Fig. 2, left side. We note that the effect of the departure of f_2^* from ε is strongest at low ε and low n.

The evaluation of the second moment in the q variable yields

$$\int q\,dq\,d\alpha\, q^2 f(q,\alpha) = \frac{1+(n-1)\varepsilon^2}{n}. \tag{2.13}$$

From Eqs. (2.11,2.13) we can now obtain the variance of the distribution of the variable-axes moment. Again, a simple formula follows for the case $\varepsilon = 0$, where $\mathrm{var}(f_2^*) = (1-\frac{\pi}{4})/n$. The scaled variance and scaled standard deviation are

$$\frac{\mathrm{var}(f_2^*)}{f_2^*} = \frac{\frac{2}{\sqrt{\pi}} - \frac{\sqrt{\pi}}{2}}{\sqrt{n}}, \qquad \frac{\sigma(f_2^*)}{f_2^*} = \sqrt{\frac{4}{\pi} - 1} \simeq 0.523, \quad (\varepsilon = 0). \tag{2.14}$$

Note that in this case there is no dependence of the scaled standard deviation on n. The case of general ε obtained numerically for various values of n is shown in Fig. 2, right side. According to Eq. (2.14), all curves approach the limit $\sqrt{\frac{4}{\pi} - 1}$ as $\varepsilon \to 0$. At the other end, in the limit of $n\varepsilon^2 \to \infty$ we have the expansions $f_2^* = \varepsilon + 1/(4\varepsilon n) + \ldots$ and $\sigma(f_2^*)/f_2^* = [1/(2\varepsilon) - \varepsilon]/n + \ldots$.

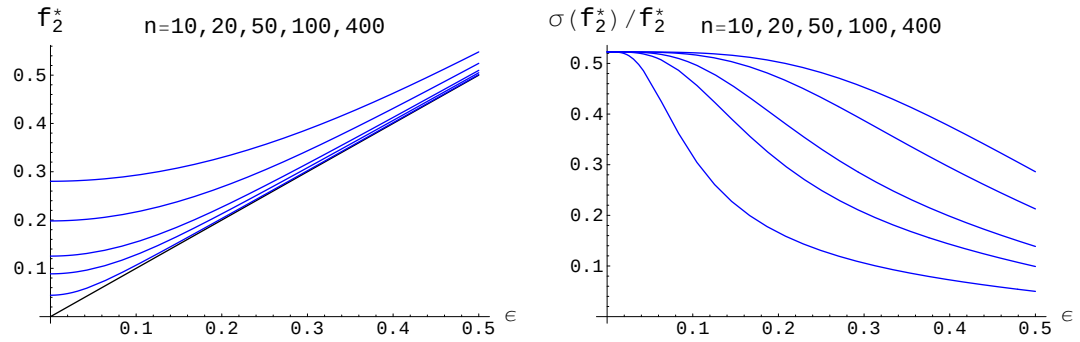

Figure 2: Toy model. Left: Dependence of the variable-axes moment f_2^* on the fixed-axes harmonic moment ε for several values of the number of particles n. As n increases, we pass from top to bottom with the presented curves. The straight line is the $n \to \infty$ limit, *i.e.* $f_2^* = \varepsilon$. Right: the same for the scaled standard deviation.

3. The general case

In the general case the analysis can be carried out in full analogy to the toy model [1]. For simplicity, in our analytic study we neglect correlations between locations of sources. If such correlations are strong, their analytic inclusion is difficult and one has to resort to numerical simulations such as those presented below. Compared to the toy model, the full two-dimensional case involves the fixed-axes moments $I_{k,l} = \int_0^\infty 2\pi\rho d\rho\, f_l(\rho)\rho^k/n$, where n is the number of sources. We have chosen the normalization $\int_0^\infty 2\pi\rho d\rho\, f_0(\rho) = n$. Generally, in analogy to Eq. (2.11)

$$\varepsilon^* = \frac{\sqrt{2}\sigma_{\bar{Y}_2}^2}{I_{k,0}\sqrt{\pi}\sigma_{X_2}} \sum_{m=0}^{\infty} (2\delta\sigma_{\bar{Y}_2}^2)^m \frac{\Gamma\left(m+\frac{1}{2}\right)\Gamma\left(m+\frac{3}{2}\right)\, {}_1F_1\left(-\frac{1}{2}; m+1; -\frac{\bar{Y}_2^2}{2\sigma_{\bar{Y}_2}^2}\right)}{m!^2}, \tag{3.1}$$

where

$$\bar{Y}_2 = I_{k,2},\ \ \sigma_{\bar{Y}_2}^2 = \frac{1}{2n}(I_{2k,0} - 2I_{k,2}^2 + I_{2k,4}),\ \ \sigma_{X_2}^2 = \frac{1}{2n}(I_{2k,0} - I_{2k,4}),\ \ \delta = \frac{1}{2\sigma_{\bar{Y}_2}^2} - \frac{1}{2\sigma_{X_2}^2}. \tag{3.2}$$

For the special case of central collisions we have the very simple results

$$\varepsilon^* = \frac{\sqrt{\pi I_{2k,0}}}{2I_{k,0}\sqrt{n}}, \qquad \frac{\sigma(\varepsilon^*)}{\varepsilon^*} = \sqrt{\frac{4}{\pi} - 1} \simeq 0.523, \qquad (b = 0). \tag{3.3}$$

Since correlations between the location of sources effectively reduce the number of sources n, they lead to an increase of ε^*, but keep its n-independent scaled variance practically constant, as shown by the simulations of the next Section. Ref. [1] contains more discussion.

4. Numerical simulations in various Glauber models

We have studied a few variants of Glauber-like models. In the standard wounded-nucleon model [15] the weight $w = 1/2$ is attributed to the point in the transverse plane at the position of the wounded nucleon. The wounding cross section is 42 mb. For binary collisions the weight $w = 1$ is

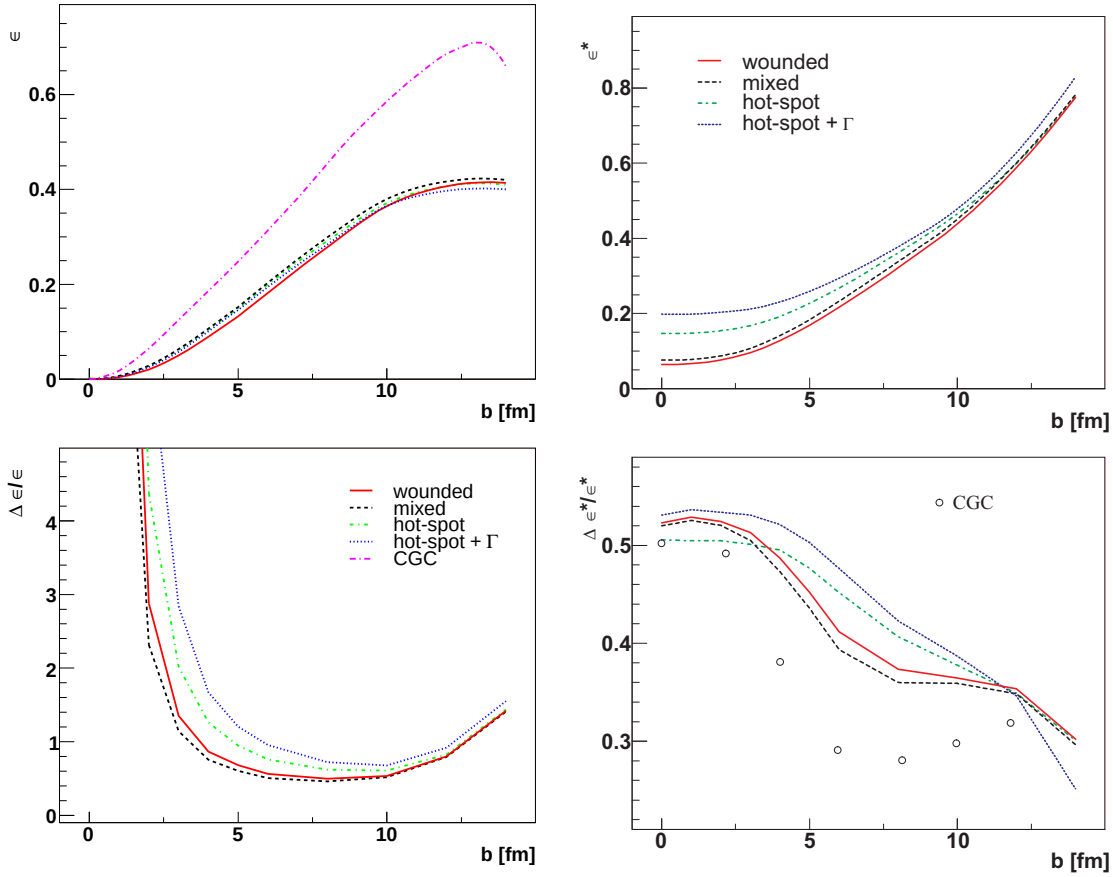

Figure 3: Left: The moment ε and its scaled standard deviation for the analyzed models plotted as functions of the impact parameter. Gold-gold collisions. Right: the same for ε^*. The results for the color-glass condensate come from Ref. [14] (dot-dashed line in top left figure) and Ref. [20] (circles in lower right figure).

attributed to each collision point. We remark that only relative magnitude of weights is important in studies of fluctuations. A successful description of the RHIC multiplicities has been achieved with a *mixed* model, amending wounded nucleons with some admixture of binary collisions [16, 17]. Then the wounded nucleon obtains the weight $w = (1-\alpha)/2$, and the binary collision the weight $w = \alpha$. The total weight averaged over events is then $(1-\alpha)N_{\rm w}/2 + \alpha N_{\rm bin}$. The fits to particle multiplicities of Ref. [17] give $\alpha = 0.145$ at $\sqrt{s_{NN}} = 200$ GeV. We also consider a model with *hot spots* in the spirit of Ref. [18], assuming that the cross section for a semi-hard binary collisions producing a hot-spot is tiny, $\sigma_{\rm hot-spot} = 0.5$ mb, however when such a rare collision occurs it produces on the average a very large amount of the transverse energy equal to $\alpha\sigma_{\rm w}/\sigma_{\rm hot-spot}$. Each source from the previously described models deposits the transverse energy with a certain probability distribution. To incorporate this effect, we superimpose the Γ distribution, multiplying the weights of the considered model with the randomly distributed number from the gamma distribution $g(w,\kappa) = w^{\kappa-1}\kappa^{\kappa}\exp(-\kappa w)/\Gamma(\kappa)$. Here we do this superposition on the hot-spot model, labeled *hot-spot*+Γ. Thus, we take the weights $(1-\alpha)g(w,\kappa)/2$ for the wounded nucleons and $\alpha g(w,\kappa)\sigma_{\rm w}/\sigma_{\rm hot-spot}$ for the binary collisions. We set $\kappa = 0.5$, which gives ${\rm var}(w) = 5$. The four

considered models (wounded-nucleon, mixed, hot-spot, and hot-spot+Γ) differ substantially by the number of sources and the amount of the built-in fluctuations.

We observe that in all four models ε is practically independent of the model (top left panel of Fig. 3). On the other hand, the scaled standard deviation (lower left panel of Fig. 3) displays a strong dependence on the model at low values of b, with the hot-spot+Γ model yielding about twice as much as the mixed model. We also notice a very strong dependence on b. At $b = 0$ the curves diverge due to dividing by the vanishing value of ε. The fluctuations are larger in models effectively having the lower number of sources, which is obvious from the statistical point of view.

As already noted in Refs. [14, 19], the value of ε obtained with the color glass condensate (CGC) is substantially higher than in all Glauber-like models reported here (upper curve in the left top panel of Fig. 3).

The harmonic moment ε^* and its scaled standard deviation are show on the right side of Fig. 3 We observe a strong model dependence of ε^* at low values of b, with models having effectively lower number of sources yielding higher values. At $b = 0$ the hot-spot+Γ model yields three times more than the wounded-nucleon model. For all models the scaled standard deviation is close to the value 0.5 for central collisions (in agreement with the results (3.3)) and drops to about 0.3 at $b = 14$ fm. At intermediate values of b the relative difference in $\sigma(\varepsilon^*)/\varepsilon^*$ between various considered models is at the level of 10-15%, which is not a very strong effect. The CGC result of Ref. [20] is lower than in the Glauber models (circles in the right bottom panel of Fig. 3).

The harmonic profiles $f_l(\rho)$ and $f_l^*(\rho)$ are displayed in Ref. [1]

5. Jet quenching

We have used the model of Refs. [21, 22] of the jet energy loss in order to explore the role of the event-by-event rotated absorbing medium. In order to take into account the variable-axes geometry, we use $f^*(\rho,\phi)$ as the density of the scattering centers for the propagating parton. The

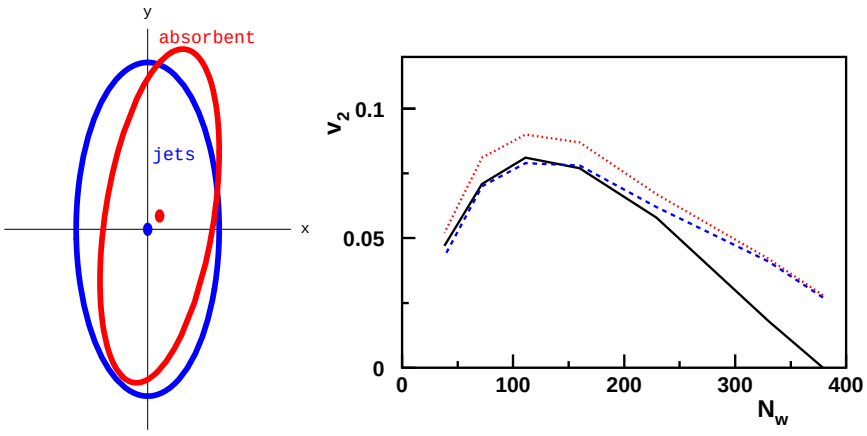

Figure 4: Left: the variable axes geometry of the absorbent vs. the fixed-axes geometry of the jet production point. Right: v_2 at high p_T as a function of the number of wounded nucleons, obtained with the variable-axes density $f^*(\rho)$ for the hot-spot scenario (dashed line), and with the fixed-axes density of the wounded nucleons $f(\rho)$ (solid line). The dotted line represents the result for the variable-axes density but without the shift and rotation of the opaque medium.

rare jet production event is distributed according to the fixed-axes profile, see Fig. (4), left side. The resulting increase of the eccentricity of the absorbent is expected to increase the asymmetry of the jet absorption. A very similar effect has been discussed for profiles calculated in the CGC model [23], where an increase in v_2 by about $10-15\%$ has been found. The absorbing medium formed in each event is rotated and also shifted. The elliptic flow (see Fig. 4, right side) at centralities larger than 20% calculated with the wounded-nucleon model in the fixed-axes frame (solid line), which serves as a reference, comes out similar to the result of the hot-spot model in the variable-axes frame (dashed line). Only if the shift and rotation of the opaque medium were neglected (dotted line) the modification of the shape leads to an increase of the high p_T elliptic flow coefficient v_2 by about $10-15\%$. The cancellation of the effects of the increased eccentricity of the medium and of the shift and rotation happens also for the other considered models (at larger centralities). The rotation of the absorbing medium yields about 2/3, and the shift about 1/3 of the total cancellation effect.

6. Fluctuations of the elliptic flow

The fluctuations of the elliptic flow, which are an important probe of the nature of the early-stage dynamics of the system [24], have recently been measured at RHIC [10, 11, 12]. The experimental procedure used in these analyses identifies the elliptic flow coefficient with the variable axes v_2, here denoted as v_2^*. The relevance of studies of fluctuations of the initial shape comes from the well-known fact that for small elliptic asymmetry one expects on hydrodynamic grounds the relation

$$\frac{\sigma(v_2^*)}{v_2^*} = \frac{\sigma(\varepsilon^*)}{\varepsilon^*}. \tag{6.1}$$

As argued in Ref. [25], the result (6.1) indicates that the mean free path in the matter created in the initial stages of the heavy-ion collisions is very small, although turbulence does not develop.

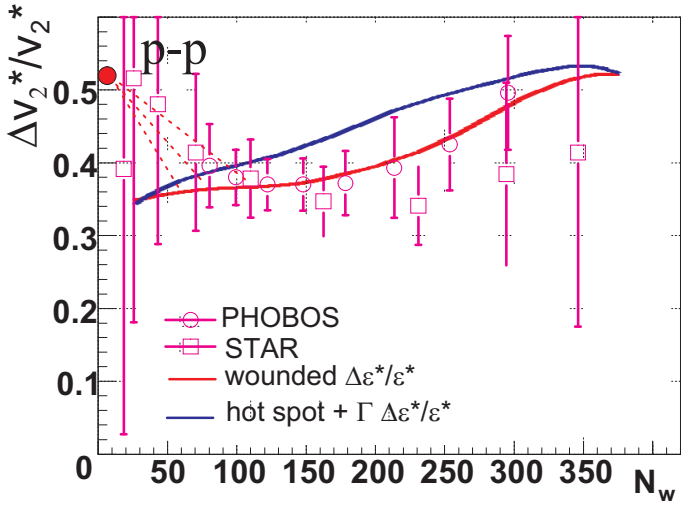

Figure 5: Fluctuations of v_2^* from the Glauber approach. Data from Refs. [10, 11, 12].

Comparison of the data to our Glauber calculations is made in Fig. 5. For central collisions we expect

$$\frac{\sigma(v_2^*)}{v_2^*}(b=0) \simeq \frac{\sigma(\varepsilon^*)}{\varepsilon^*}(b=0) \simeq \sqrt{\frac{4}{\pi}-1} \simeq 0.52, \tag{6.2}$$

which is compatible to the data, although the error bars are large.

Amusingly, the limiting value of Eq. (6.2) is also obtained for peripheral collisions, if these form a collection of several independent pp collisions (of course, no hydro here). In each such collision particles are emitted with a certain momentum distribution, which is cylindrically symmetric. Thus, the same effect as discussed for the shape fluctuations occurs for the momentum fluctuations. In other words, we replace the coordinates with momenta in our analysis, and get $\sigma(v_2^*)/v_2^*(\text{peripheral}) \simeq 0.52$. This value is represented by a blob in Fig. 5. Some transition from hydro to independent pp collisions must occur, which is indicated by the interpolating dashed lines in the figure.

We end this talk with some comments on the derivation of Eq. (6.1) as well as on higher-harmonic probes. Perturbation theory applied to smooth (*i.e.* linearization is sensible) hydrodynamics together with hierarchy of relaxation times for subsequent harmonics, *e.g.* $\tau_2 \gg \tau_4$, leads to further results [1]. In particular,

$$v_4^* \sim \varepsilon^{*2} \sim v_2^{*2}. \tag{6.3}$$

In Ref. [27] the variable v_4/v_2^2 has been suggested as a sensitive probe of the hydrodynamic evolution. The simulations of Refs. [26, 27] show that with increasing time the value of v_2 saturates, while v_4 quickly assumes the value proportional to v_2^2, supporting the assumption $\tau_2 \gg \tau_4$ used in the above argumentation. For the fluctuations one gets immediately from Eq. (6.3) the prediction

$$\frac{\sigma(v_4^*)}{v_4^*} = 2\frac{\sigma(v_2^*)}{v_2^*}. \tag{6.4}$$

Relation (6.4), if verified experimentally, would support the scenario of smooth hydro evolution with the mentioned hierarchy of scales. On similar grounds, for the azimuthal Hanbury-Brown–Twiss (HBT) correlation radius, $R^{\rm HBT}(\phi)$, one expects

$$R_4^{\rm HBT} \sim (R_2^{\rm HBT})^2, \tag{6.5}$$

where $R^{\rm HBT}(\phi) = R_0^{\rm HBT} + 2R_2^{\rm HBT}\cos(2\phi) + 2R_4^{\rm HBT}\cos(4\phi) + \ldots$.

7. Conclusions

Here are our main points:

- We have analyzed four Glauber-like models, with different degree of fluctuation: the wounded-nucleon model, the mixed model, the hot-spot model, and the hot-spot model with the superimposed Γ distribution.

- We have obtained numerically the fixed-axes and variable-axes harmonic profiles [1] and analyzed their moments. The variable-axes moments ε^*, and the fixed-axes scaled standard deviation $\sigma(\varepsilon)/\varepsilon$ are sensitive to the choice of the model, while $\sigma(\varepsilon^*)/\varepsilon^*$ is not, changing at most by 10-15% from model to model at intermediate values of b.

- Analytic formulas explain certain features of the simulations, in particular, they show that at $b = 0$ the multiple-axes scaled variances are close to the value 0.5, insensitive of the model used, the collision energy, the mass number of the colliding nuclei, or the number of particle sources. The behavior of $\sigma(\varepsilon^*)/\varepsilon^*$ at low b is thus largely *governed by the statistics*

- Fixed-reaction-plane experimental analyses would reveal more information on the system and would allow to discriminate the theoretical predictions, as fluctuations of ε are sensitive to the chosen model.

- For the jet v_2 we find that the effect of the increased variable-axes eccentricity is largely canceled by the shift of the center of mass and the rotation of the principal axes of the absorbing medium. This leads to practically no change of the jet emission asymmetry at intermediate and large impact parameters. Only at small b the increase of the deformation takes over the relatively less important shift and rotation.

- On hydrodynamic grounds, the analysis of the variable-axes moments in the coordinate space carries over to the collective flow and analysis of v_2^*. In particular, Eq. (6.2) holds for the variable-axes elliptic flow coefficient at central collisions.

- The same value is also obtained for peripheral collisions, since these consist of of several independent pp collisions. In each such collision particles are emitted from a cylindrically symmetric momentum distribution. Replacing coordinates with momenta in our analysis yields to $\sigma(v_2^*)/v_2^*(\text{peripheral}) \simeq 0.52$. Thus, statistics fixes the two end-point values in Fig. 6.2.

- Under assumptions of smoothness, perturbation theory made on top of azimuthally symmetric hydro leads to sensitivity of higher-harmonic late-time measures, v_4^*, $R_4^{\rm HBT}$, *etc.*, to the initial *quadrupole* deformation $\varepsilon^*(t_0)$ only. Higher harmonics of the initial shape deformation are irrelevant, as they presumably are damped fast. A number of relations follows for various measures and their event-by-event fluctuations, *e.g.* Eq. (6.4).

- It would be a challenge to measure the v_4^* fluctuations and test the smooth hydro assumption by verifying relation (6.4).

One of us (WB) thanks Paul Sorensen, Constantin Loizides, and Wit Busza for useful discussions concerning the experimental determination of v_2 and its fluctuations.

References

[1] W. Broniowski, P. Bożek, and M. Rybczyński (2007), `nucl-th/0706.4266`.

[2] C. E. Aguiar, T. Kodama, T. Osada, and Y. Hama, J. Phys. **G27**, 75 (2001).

[3] C. E. Aguiar, Y. Hama, T. Kodama, and T. Osada, Nucl. Phys. **A698**, 639 (2002).

[4] M. Miller and R. Snellings (2003), `nucl-ex/0312008`.

[5] R. S. Bhalerao, J.-P. Blaizot, N. Borghini, and J.-Y. Ollitrault, Phys. Lett. **B627**, 49 (2005).

[6] R. Andrade, F. Grassi, Y. Hama, T. Kodama, and O. Socolowski, Jr., Phys. Rev. Lett. **97**, 202302 (2006).

[7] S. A. Voloshin (2006), `nucl-th/0606022`.

[8] S. A. Voloshin, A. M. Poskanzer, A. Tang, and G. Wang (2007), `nucl-th/0708.0800`.

[9] B. Alver et al. (PHOBOS), PoS **CFRNC2006**, 023 (2006).

[10] B. Alver et al. (PHOBOS) (2006), `nucl-ex/0610037`.

[11] P. Sorensen (STAR) (2006), `nucl-ex/0612021`.

[12] B. Alver et al. (PHOBOS) (2007), `nucl-ex/0701049`.

[13] A. M. Poskanzer and S. A. Voloshin, Phys. Rev. **C58**, 1671 (1998).

[14] T. Hirano, U. W. Heinz, D. Kharzeev, R. Lacey, and Y. Nara, Phys. Lett. **B636**, 299 (2006).

[15] A. Białas, M. Błeszyński, and W. Czyż, Nucl. Phys. **B111**, 461 (1976).

[16] B. B. Back et al. (PHOBOS), Phys. Rev. **C65**, 031901 (2002).

[17] B. B. Back et al. (PHOBOS), Phys. Rev. **C70**, 021902 (2004).

[18] M. Gyulassy, D. H. Rischke, and B. Zhang, Nucl. Phys. **A613**, 397 (1997).

[19] H. J. Drescher and Y. Nara, Phys. Rev. **C75**, 034905 (2007).

[20] H.-J. Drescher and Y. Nara (2007), `nucl-th/0707.0249`.

[21] A. Drees, H. Feng, and J. Jia, Phys. Rev. **C71**, 034909 (2005).

[22] W. A. Horowitz, Acta Phys. Hung. **A27**, 221 (2006).

[23] H.-J. Drescher, A. Dumitru, A. Hayashigaki, and Y. Nara, Phys. Rev. **C74**, 044905 (2006).

[24] S. Mrówczyński and E. V. Shuryak, Acta Phys. Polon. **B34**, 4241 (2003).

[25] S. Vogel, G. Torrieri, and M. Bleicher (2007), `nucl-th/0703031`.

[26] P. F. Kolb, Phys. Rev. **C68**, 031902 (2003).

[27] N. Borghini and J.-Y. Ollitrault, Phys. Lett. **B642**, 227 (2006).